

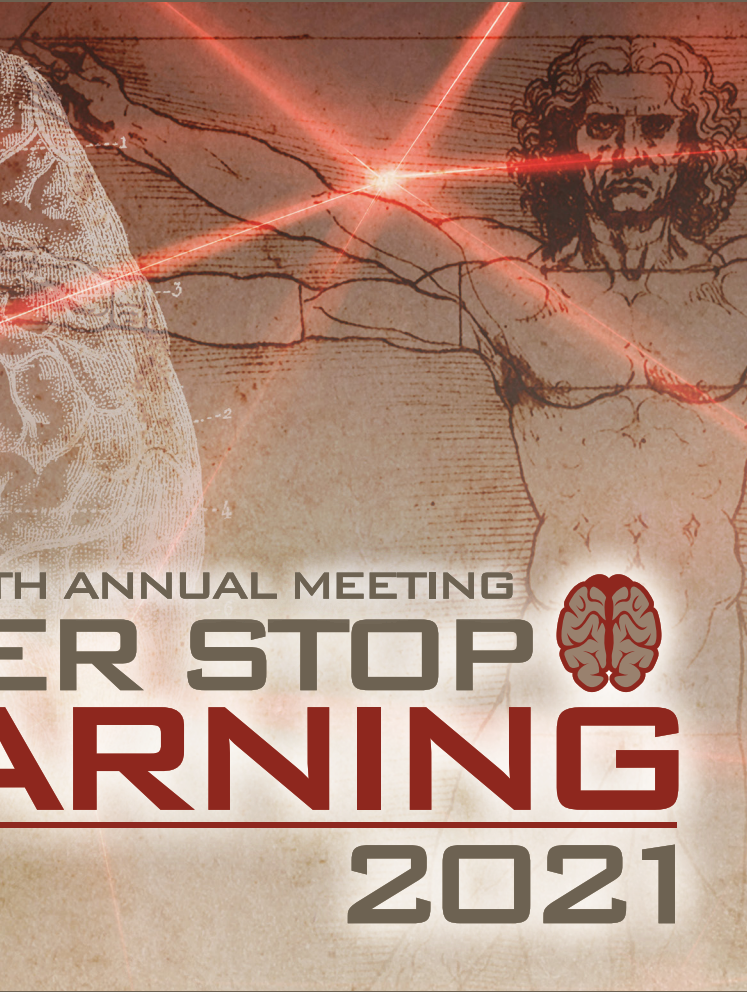
# LI

## LABORATORY INVESTIGATION

THE BASIC AND TRANSLATIONAL PATHOLOGY RESEARCH JOURNAL

# ABSTRACTS

## GENERAL SURGICAL PATHOLOGY (405-421)



USCAP 110TH ANNUAL MEETING  
**NEVER STOP  
LEARNING**  
2021

MARCH 13-18, 2021

VIRTUAL AND INTERACTIVE

Published by  
**SPRINGER NATURE**  
[www.ModernPathology.org](http://www.ModernPathology.org)

 **USCAP** AN OFFICIAL JOURNAL OF THE  
UNITED STATES AND CANADIAN  
ACADEMY OF PATHOLOGY  
Creating a Better Pathologist

**EDUCATION COMMITTEE**

**Jason L. Hornick**  
Chair

**Rhonda K. Yantiss, Chair**  
Abstract Review Board and Assignment Committee

**Kristin C. Jensen**  
10 Chair, CME Subcommittee

**Laura C. Collins**

Interactive Microscopy Subcommittee

**Raja R. Seethala**  
Short Course Coordinator

**Ilan Weinreb**  
Subcommittee for Unique Live Course Offerings

**David B. Kaminsky**  
(Ex-Officio)  
**Zubair W. Baloch**  
**Daniel J. Brat**  
**Sarah M. Dry**  
**William C. Faquin**  
**Yuri Fedoriw**  
**Karen Fritchie**  
**Jennifer B. Gordetsky**  
**Melinda Lerwill**  
**Anna Marie Mulligan**

**Liron Pantanowitz**  
**David Papke,**  
Pathologist-in-Training  
**Carlos Parra-Herran**  
**Rajiv M. Patel**  
**Deepa T. Patil**  
**Charles Matthew Quick**  
**Lynette M. Sholl**  
**Olga K. Weinberg**  
**Maria Westerhoff**  
**Nicholas A. Zoumberos,**  
Pathologist-in-Training

**ABSTRACT REVIEW BOARD**

**Benjamin Adam**  
**Rouba Ali-Fehmi**  
**Daniela Allende**  
**Ghassan Allo**  
**Isabel Alvarado-Cabrero**  
**Catalina Amador**  
**Tatjana Antic**  
**Roberto Barrios**  
**Rohit Bhargava**  
**Luiz Blanco**  
**Jennifer Boland**  
**Alain Borczuk**  
**Elena Brachtel**  
**Marilyn Bui**  
**Eric Burks**  
**Shelley Caltharp**  
**Wenqing (Wendy) Cao**  
**Barbara Centeno**  
**Joanna Chan**  
**Jennifer Chapman**  
**Yunn-Yi Chen**  
**Hui Chen**  
**Wei Chen**  
**Sarah Chiang**  
**Nicole Cipriani**  
**Beth Clark**  
**Alejandro Contreras**  
**Claudiu Cotta**  
**Jennifer Cotter**  
**Sonika Dahiya**  
**Farbod Darvishian**  
**Jessica Davis**  
**Heather Dawson**  
**Elizabeth Demicco**  
**Katie Dennis**  
**Anand Dighe**  
**Suzanne Dintzis**  
**Michelle Downes**

**Charles Eberhart**  
**Andrew Evans**  
**Julie Fanburg-Smith**  
**Michael Feely**  
**Dennis Firchau**  
**Gregory Fishbein**  
**Andrew Folpe**  
**Larissa Furtado**  
**Billie Fyfe-Kirschner**  
**Giovanna Giannico**  
**Christopher Giffith**  
**Anthony Gill**  
**Paula Ginter**  
**Tamar Giorgadze**  
**Purva Gopal**  
**Abha Goyal**  
**Rondell Graham**  
**Alejandro Gru**  
**Nilesh Gupta**  
**Mamta Gupta**  
**Gillian Hale**  
**Suntrea Hammer**  
**Malini Harigopal**  
**Douglas Hartman**  
**Kammi Henriksen**  
**John Higgins**  
**Mai Hoang**  
**Aaron Huber**  
**Doina Ivan**  
**Wei Jiang**  
**Vickie Jo**  
**Dan Jones**  
**Kirk Jones**  
**Neerja Kambham**  
**Dipti Karamchandani**  
**Nora Katabi**  
**Darcy Kerr**  
**Francesca Khani**

**Joseph Khoury**  
**Rebecca King**  
**Veronica Klepeis**  
**Christian Kunder**  
**Steven Lagana**  
**Keith Lai**  
**Michael Lee**  
**Cheng-Han Lee**  
**Madelyn Lew**  
**Faqian Li**  
**Ying Li**  
**Haiyan Liu**  
**Xiuli Liu**  
**Lesley Lomo**  
**Tamara Lotan**  
**Sebastian Lucas**  
**Anthony Magliocco**  
**Kruti Maniar**  
**Brock Martin**  
**Emily Mason**  
**David McClintock**  
**Anne Mills**  
**Richard Mitchell**  
**Neda Moatamed**  
**Sara Monaco**  
**Atis Muehlenbachs**  
**Bitu Naini**  
**Dianna Ng**  
**Tony Ng**  
**Michiya Nishino**  
**Scott Owens**  
**Jacqueline Parai**  
**Avani Pendse**  
**Peter Pytel**  
**Stephen Raab**  
**Stanley Radio**  
**Emad Rakha**  
**Robyn Reed**

**Michelle Reid**  
**Natasha Rekhman**  
**Jordan Reynolds**  
**Andres Roma**  
**Lisa Rooper**  
**Avi Rosenberg**  
**Esther (Diana) Rossi**  
**Souzan Sanati**  
**Gabriel Sica**  
**Alexa Siddon**  
**Deepika Sirohi**  
**Kalliopi Siziopikou**  
**Maxwell Smith**  
**Adrian Suarez**  
**Sara Szabo**  
**Julie Teruya-Feldstein**  
**Khin Thway**  
**Rashmi Tondon**  
**Jose Torrealba**  
**Gary Tozbikian**  
**Andrew Turk**  
**Evi Vakiani**  
**Christopher VandenBussche**  
**Paul VanderLaan**  
**Hannah Wen**  
**Sara Wobker**  
**Kristy Wolniak**  
**Shaofeng Yan**  
**Huihui Ye**  
**Yunshin Yeh**  
**Anjana Yeldandi**  
**Gloria Young**  
**Lei Zhao**  
**Minghao Zhong**  
**Yaolin Zhou**  
**Hongfa Zhu**

To cite abstracts in this publication, please use the following format: **Author A, Author B, Author C, et al. Abstract title (abs#). In "File Title." *Laboratory Investigation* 2021; 101 (suppl 1): page#**

**405 Head-to-Head Comparison of S-100 and SOX10 in the Diagnosis of Melanoma**

Ibrahim Abukhiran<sup>1</sup>, Ilham Farhat<sup>1</sup>, Andrew Bellizzi<sup>1</sup>, Sarag Boukhar<sup>1</sup>

<sup>1</sup>University of Iowa Hospitals & Clinics, Iowa City, IA

**Disclosures:** Ibrahim Abukhiran: None; Ilham Farhat: None; Andrew Bellizzi: None; Sarag Boukhar: None

**Background:** S-100 has a long history as the "gold-standard" melanoma screening marker, though SOX10 has emerged as an alternative in this diagnostic setting. Based on anecdotal experience with SOX10-positive/S-100-weak-to-negative melanomas identified in the workup of high-grade tumors of uncertain lineage, one of us has switched to screening with SOX10. We performed a head-to-head comparison in a large cohort of well-annotated melanomas.

**Design:** S-100 and SOX10 immunohistochemistry (IHC) were performed on tissue microarrays (TMAs) of 273 melanoma cases from 248 patients. These included 137 primaries (90% skin, 5% sinonasal, 5% other mucosal sites) and 136 metastases. BAP1 and BRAF V600E mutation-specific IHC had been previously performed. IHC-stained slides were digitally scanned (3DHISTECH; Budapest, Hungary) and whole TMA cores were annotated. 3DHISTECH QuantCenter nuclear (SOX10) and membranous (S-100) algorithms were optimized to identify immunoreactive tumor cells (ITCs) and run on annotations. H&E whole slide images were visualized for rare cases showing low H-scores (<10) to confirm positivity or negativity. A digitally analyzed H-score was determined according to the following formula: H-Score= [(strong ITC% X 3) + (moderate ITC% X 2) + (weak ITC% X 1)]. Fisher's exact and Mann Whitney tests and one-way ANOVA were used with p<0.05 considered significant.

**Results:** SOX10-positivity was identified in 99.3% (267 of 269) of cases with a mean (95% CI) and standard deviation (SD) of 179 (169-188) and 77, while only 95% (258 of 270) were S-100-positive with a mean (95% CI) and SD of 223 (213-232) and 78. Both SOX10-negative cases were also S-100-negative (a cutaneous superficial spreading melanoma and a lung metastasis from desmoplastic melanoma). In total, the 13 S-100-negative tumors were of cutaneous (6), sinonasal (3), ocular (2), and mucosal (2) origin. SOX10 H-scores were higher in primaries, in patients without synchronous/metachronous metastasis, and in BRAF V600E-negative tumors. S-100 was weaker in female patients and in ocular/sinonasal primaries. Refer to the Table for detailed results.

Association of SOX10 and S100 Positivity to Clinicopathologic Variables							
		S100+ n (%)	p	Average S100 H-Score	p	Average SOX10 H-Score	p
Tissue	Metastatic	130 (96)	0.84	208	0.30	165	<b>0.0017</b>
	Primary	127 (95)		207		181	
Clinical metastasis	No	30 (100)	0.92	212	0.39	183	<b>0.0167</b>
	Yes	70 (99)		205		166	
Gender	F	111 (93)	0.92	195	<b>0.0141</b>	178	0.13
	M	146 (97)		218		169	
Location	Cutaneous	221 (97)	0.8	215	0.04	180	0.7
	Noncutaneous	32 (82)		207		172	
BAP1	Intact	250 (96)	0.9	223	0.5	178	0.16
	Lost	7 (78)		237		218	
BRAF V600E	Negative	182 (94)	0.9	225	0.5	188	<b>0.0008</b>
	Positive	75 (99)		220		156	

Figure 1 - 405

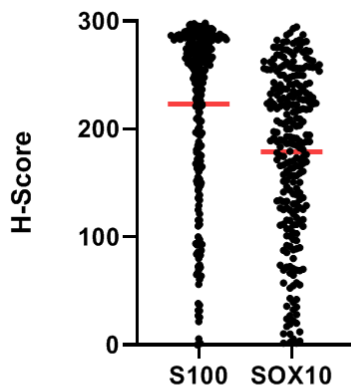


Figure-1: Scatter plot of H-score showing the different distribution patterns of SOX10 and S100. Each black dot represents one case. The red lines indicate the mean.

**Conclusions:** Compared to S-100, SOX10 was more sensitive for the diagnosis of melanoma (99.3% vs 95%), and no tumors were SOX10-negative/S-100-positive. SOX10 H-score analysis revealed several interesting correlates, including stronger expression in primaries, in patients not experiencing metastasis, and in BRAF wild-type tumors.

#### 406 PRAME Protein Expression in Epithelial Tumors: An Immunohistochemical Study

Rofieda Alwaqfi<sup>1</sup>, Andrew Bellizzi<sup>1</sup>

<sup>1</sup>University of Iowa Hospitals & Clinics, Iowa City, IA

**Disclosures:** Rofieda Alwaqfi: None; Andrew Bellizzi: None

**Background:** PRAME (PReferentially expressed Antigen in MELanoma) is a melanoma-associated antigen that was found to be expressed in up to 80%-90% of melanomas while normal melanocytes and benign melanocytic neoplasms are mostly negative or have a very low-level expression of the protein. As such, PRAME immunohistochemistry is thought to be helpful in distinguishing malignant melanocytic proliferations from benign proliferations. While the TCGA pan-cancer study showed that mRNA PRAME expression is most frequent in cutaneous melanomas, other malignant neoplasms including different types of carcinomas appeared also to express PRAME mRNA in certain levels (Figure 1). In this study, we examined the immunohistochemical expression of PRAME protein in epithelial tumor and the utility of including PRAME immunohistochemical stain in the work-up of malignant neoplasms of unknown lineage.

**Design:** Tissue microarrays were constructed from available paraffin blocks of 80 carcinomas from multiple organs (68 adenocarcinomas including breast (n=11), lung (n=30), colonic (n=7), esophageal (n=5), mullerian (n=3), renal (n=7), prostatic (n=1) and adenocarcinoma of uncertain primary origin (n=4) in addition to squamous cell carcinomas (n=6), neuroendocrine carcinoma (n=1) and urothelial carcinomas (n=5)). PRAME immunohistochemistry (IHC) was performed on the included cases. Intensity (0-3+) and extent (0-100%) of expression was evaluated, and an H-score was calculated. Fisher's exact and Mann Whitney tests were used with p<0.05 considered significant.

**Results:** Nuclear PRAME staining was present in 58% (46/80) of all studied carcinomas. Of the studied adenocarcinomas, 58% (40/68) were positive with highest intensity and extent of expression noted in esophageal adenocarcinomas (100%, 5/5) (p value=0.15). More frequent nuclear expression was found in squamous cell carcinomas (83%, 5/6) compared with adenocarcinomas (58%, 40/68) (p=0.39). Of note, all urothelial carcinomas included were negative. Detailed PRAME expression data by all carcinomas studied are presented in the Table.

Carcinoma type	N	Percentage of positive cases	Mean H-score	Median H-score
All carcinomas	80	58% (46/80)	98	63
Overall adenocarcinomas	68	59% (40/68)	98	60
Breast adenocarcinomas	11	55% (6/11)	88	94
Lung adenocarcinoma	30	53% (16/30)	92	33
Colonic adenocarcinoma	7	14% (1/7)	1	1
Esophageal adenocarcinoma	5	100% (5/5)	144	200
Renal cell carcinoma	7	56% (4/7)	110	60
Ovarian adenocarcinoma	3	40% (1/3)	54	53
Prostatic adenocarcinoma	1	0	0	0
Carcinoma of unknown primary	4	75% (3/4)	124	67
Squamous cell carcinomas	6	83% (5/6)	119	73
Urothelial carcinomas	5	0	0	0

Figure 1 - 406



**Conclusions:** While PRAME IHC can be helpful in differentiating malignant melanocytic neoplasms from benign proliferations, our data suggest that its use as melanocytic lineage marker in the work-up of malignant neoplasms of uncertain nature is of limited value given its frequent expression by many epithelial tumors.

**407 Correlation of PD-L1 Expression, Clinicopathologic and Molecular Characteristics in an Array of Solid Tumors: A Large-Scale Real World Study**  
 Kanika Arora<sup>1</sup>, Harshita Mehrotra<sup>1</sup>, Kasturi Saikia<sup>1</sup>, Rand Abou Shaar<sup>1</sup>, Mohamed Alhamar<sup>1</sup>, Dhananjay Chitale<sup>2</sup>  
<sup>1</sup>Henry Ford Health System, Detroit, MI, <sup>2</sup>Henry Ford Hospital, Detroit, MI

**Disclosures:** Kanika Arora: None; Harshita Mehrotra: None; Kasturi Saikia: None; Rand Abou Shaar: None; Mohamed Alhamar: None; Dhananjay Chitale: None

**Background:** Programmed death ligand-1 (PD-L1) is a predictive marker of anti-programmed death protein 1 (PD-1)/PD-L1 therapies for solid tumors. Limited literature exists correlating PD-L1 expression, clinicopathological & molecular profiles. We aimed to 1) correlate PD-L1 immunohistochemistry (IHC) results with these profile across multiple solid tumors & 2) assess clinical outcomes (overall survival (OS) & disease-free survival (DFS)) of PD-L1 status with / without anti-PD-L1 immunotherapy (IT).

**Design:** All cases tested for PD-L1 IHC over 2 years (Aug 2019-Sep 2020) were retrieved for this study. Clinicopathological variables recorded included age, race, tumor type, type of PD-L1 clone, PD-L1 status (Tumor Proportion Score (TPS): negative: <1%, low:1-49%, high: >50%), Combined Positive Score (CPS): negative <1, low 1-10, high > 10), clinical stage, anti-PD-L1 IT. Microsatellite instability (MSI) status using IHC & Ploymerase chain reaction (PCR) assays was recorded. High PD-L1 was defined as PD-L1 expression of TPS >50%/CPS>10. Outcome studies included OS and DFS after generating Kaplan-Meier curves & compared using log rank test. Univariate analysis using Cox regression models were also used.

**Results:** There were 205 cases tested for PD-L1 by IHC. Cohort included non-small cell lung cancers (127), head & neck carcinomas (37), gastric or gastroesophageal carcinoma (20), kidney or urothelial carcinoma (16), cervical carcinomas (5). Median age was 70 years (range 28-90). Most were high stage cancers [stage 1: 5/205, stage 2: 5/205, stage 3: 30/205, stage 4 165/205]. PD-L1 IHC clones included: 22C3 (152/205), 28-8 (21/205) & both (32/205). High PD-L1 expression was observed in 52/205 (25.3%), out of which [37/127 (29.1%) were adenocarcinoma, 13/54 (24%) were squamous cell carcinoma, 2/24 (4.1%) others]. Anti PD-L1 IT was given in 65/205 (31.7%) patients. Anti PD-L1 IT was significantly associated with longer median survival OS ( $p=0.015$ ) & DFS ( $p=0.004$ ) (Figure 1). PD-L1 status was significantly associated with OS ( $p=0.034$ ) but not DFS ( $p=0.076$ ) (Figure 1). High PD-L1 had shorter median survival and higher hazards of death in OS (HR=5.4, CI-1.3-23.1) irrespective of IT. Association between three groups of PD-L1 status when compared with IT was statistically significant ( $p=0.048$ , Figure 2). PD-L1 & MSI testing was available in 29 patients & did not show any statistical correlation in this small cohort. No significant difference in survival for those received IT (4/29) vs no IT (25/29) & tested for both PD-L1 & MSI (OS:  $p=0.277$ , DFS:  $p=0.107$ ).

Figure 1 - 407

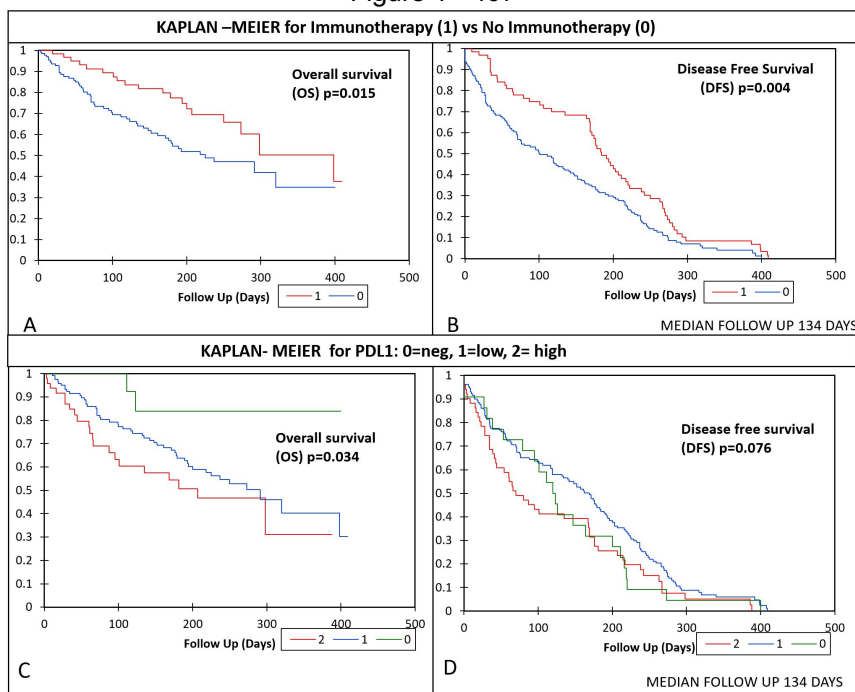


Figure 2 - 407

ANTI-PDL1 IMMUNOTHERAPY	NEGATIVE PDL1 TPS/CPS (<1%)	LOW PDL1 TPS(1-49%) CPS(1-10%)	HIGH PDL1 TPS >50% /CPS >10	TOTAL	CHI SQUARE TEST
YES	4	38	23	65	P= 0.048
NO	18	93	29	140	
TOTAL	22	131	52	205	

**Conclusions:** This study supports the rational approach for PD-L1 therapy. High PD-L1 expression is more commonly seen in adenocarcinoma. Expression of high PD-L1 is associated with worse OS but not DFS. PD-L1 IT is significantly associated with longer median survival, OS & DFS. Larger, prospective studies are needed to support our findings.

**408 Expression of PD-L1 Antibody in Anal and Cervical Invasive Squamous Cell Carcinoma: Comparison of Two Clones**

Vaidehi Avadhani<sup>1</sup>, Ashley Monsrud<sup>2</sup>, Marina Mosunjac<sup>2</sup>, Uma Krishnamurti<sup>2</sup>  
<sup>1</sup>Emory University Hospital, Atlanta, GA, <sup>2</sup>Emory University, Atlanta, GA

**Disclosures:** Vaidehi Avadhani: None; Ashley Monsrud: None; Marina Mosunjac: None; Uma Krishnamurti: None

**Background:** PD-L1 is an immunoregulatory molecule associated with adverse outcomes in several malignancies. Detection of PD-L1 by immunohistochemistry (IHC) on tumor cells is increasingly being integrated into the clinical management and for possible selection of patients who can respond to therapy. In this scenario, laboratories may have to explore which PD-L1 assays show the most reliable staining. The aim of this study was to compare the expression patterns of the commercially available Dako and Cell signaling (CS) PD-L1 antibody in anal and cervical invasive squamous cell carcinoma.

**Design:** 51 anal invasive squamous cell carcinoma cases (AISCC) and 73 cervical invasive squamous cell carcinoma (CISCC) cases were first stained using the Dako antibody (22C3 pharmDx). For AISCC, TPS was evaluated. TPS is the percentage of viable tumor cells showing positive staining. TPS= # of PD-L1 positive tumor cells/Total # of PD-L1 positive and PD-L1 negative tumor cells. For CISCC, a combined positive score (CPS) was evaluated. CPS = # PD-L1 staining cells (tumor cells, tumoral and peritumoral lymphocytes, macrophages) X 100/Total # of viable tumor cells. A subset (55 cases) was selected for comparison with the CS antibody (clone E1L3N, 1: 200 dilution). Cases stained by CS antibody included 10 cases of AISCC and 10 cases of CISCC that were PD-L1 negative by the Dako, antibody, the rest (35 cases) being PD-L1+ by Dako.

**Results:** See Table 1.

Anal ISCC: 18/51 (35%) of AISCC were PD-L1+ by the Dako antibody (Fig 1). By CS antibody (Fig 2), PD-L1 was positive in 40% of the Dako PD-L1+ cases. Six PD-L1+ cases with low TPS (1-10) by Dako were negative by CS antibody. Seven PD-L1+ cases with intermediate TPS (12-45) by Dako were positive but with lower TPS (1-20) by CS antibody.

Cervical ISCC: 30/73 (41%) of CISCC were PD-L1+ by the Dako antibody. By CS antibody, PD-L1 was positive in 35% of Dako PD-L1+ cases. Cases with lower CPS by the Dako antibody were seen to be negative by CS antibody. In cases PD-L1 + by the CS antibody, CPS scores were lower by the CS antibody compared with the Dako antibody.

Both in AISCC and CISCC, compared with the Dako antibody (Fig 1) cases that were PD-L1+ by the CS antibody had a lower intensity of staining (Fig 2).

All cases (10 AISCC and 10 CISCC) with no PD-L1 expression by the Dako antibody were also negative by the CS antibody.

ISCC	Dako PDL1 +	CS PDL1 +
Anal ISCC (15)	15	6/15 (40%)
Cervical ISCC (20)	20	7/20 (35%)

Figure 1 - 408

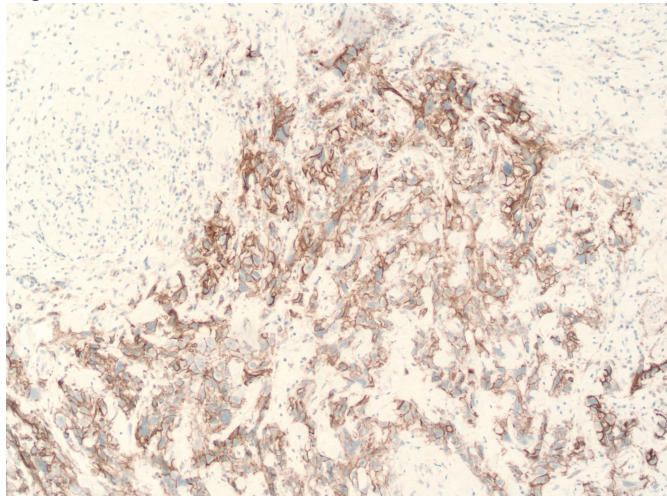
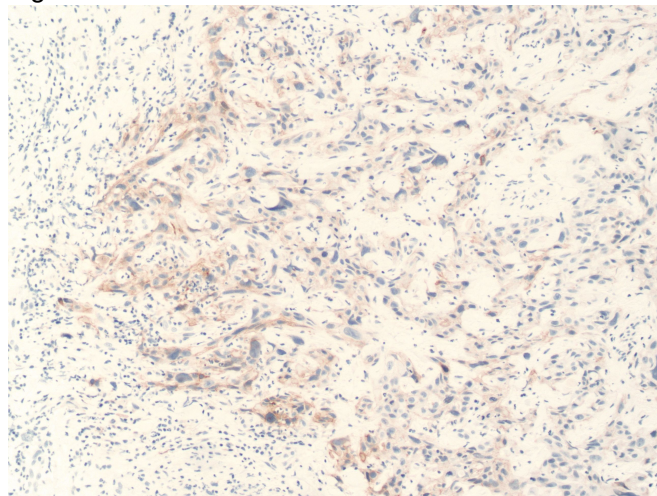


Figure 2 - 408



**Conclusions:** Various antibody clones show variable staining patterns and a detailed study of their expression patterns may be essential in order to make the appropriate choice for patients. In anal and cervical ISCC, the CS PD-L1 antibody (clone E1L3N), although equally specific, was seen to be less sensitive than the Dako PD-L1 (22C3 pharmDx) antibody.

**409 Clinico-Pathologic Findings in Patients with Median Arcuate Ligament Syndrome: A Case Series**

Manita Chaum<sup>1</sup>, Daniel Shouhed<sup>1</sup>, Stacey Kim<sup>2</sup>, Alberto Marchevsky<sup>1</sup>

<sup>1</sup>Cedars-Sinai Medical Center, West Hollywood, CA, <sup>2</sup>Cedars-Sinai Medical Center, Los Angeles, CA

**Disclosures:** Manita Chaum: None; Daniel Shouhed: *Consultant*, Intuitive; Stacey Kim: None; Alberto Marchevsky: None

**Background:** Median arcuate ligament syndrome (MALS), also known as Dunbar syndrome or Celiac Artery Compression Syndrome, is a rare entity characterized by the development of post-prandial epigastric pain that can be quite severe and is respiratory-dependent, nausea, vomiting, weight loss resulting from sitophobia and other vague abdominal symptoms. It is more prevalent in young women. MALS' patients have been reported in the surgical literature in case reports and small case series. It remains controversial whether the symptoms are secondary to ligament compression of the celiac artery or neurogenic. To our knowledge, there are no studies in the pathology literature describing the pathologic changes seen in these patients.

**Design:** The clinical, imaging and pathologic findings of 4 patients operated for MALS at Cedars-Sinai Medical Center from 2000-2020 are described. A systematic review of English literature was performed using the PubMed engine of the National Library of Medicine and the keywords "median arcuate ligament syndrome", "Dunbar syndrome" and "celiac artery compression syndrome."

**Results:** All patients were female with a median age 32.5 (range 25-55 years), and a median BMI of 23.5 kg/m<sup>2</sup>. Patients presented with chronic abdominal pain (4/4), nausea (3/4), emesis (2/4), non-bloody diarrhea (1/4), loss of appetite (1/4), and weight loss (1/4). All four patients underwent either robotic or laparoscopic surgery. Intraoperative exploration showed that the ligament was present in an abnormal location encasing the celiac axis



and adjacent nerves and ganglia (Fig. 1). Four patients underwent median arcuate ligament division and nerve plexus excision. Symptoms improved in all patients. Surgical specimens showed fibroadipose tissue with small nerves in 3 of the 4 specimens and a nerve plus ganglion in 1 case (Table 1). The resected nerves showed an early traumatic neuroma in one case and mild perineural fibrosis in 3 other cases shown by H&E and Trichrome stains (Fig. 2). 211 patients have been reported in the surgical literature. Only the study by Klimas et al demonstrated histopathologic findings in a patient.

Case	Age	Gender	BMI (kg/m <sup>2</sup> )	Pre-operative symptoms	Radiology	Histology	Post-operative symptoms
1	25	F	28	Severe episodic epigastric pain aggravated with food  Nausea  Loss of appetite	Celiac trunk with poststenotic dilation   Mild celiac stenosis	Mild perineural fibrosis and ganglion	Resolution of abdominal pain
2	55	F	28	History of Crohn's disease  Abdominal pain, nausea, emesis, non-bloody diarrhea	Severe narrowing at celiac artery origin  Greater than 60% diameter reduction (greater than 70% stenosis) of the celiac artery. The velocities in the celiac artery remained abnormal respiration.	Mild perineural fibrosis	Improved abdominal pain
3	26	F	19	History of Crohn's disease  Chronic post-prandial abdominal pain  Nausea  Emesis	Unremarkable celiac artery  Pain resolved with plexus nerve block	Mild perineural fibrosis	Improved abdominal pain, nausea and emesis
4	39	F	18	Generalized abdominal pain requiring narcotics  20lb weight loss	Mild narrowing of the proximal celiac artery with poststenotic dilatation	Early traumatic neuroma	Improved pain, not requiring narcotics

Figure 1 - 409

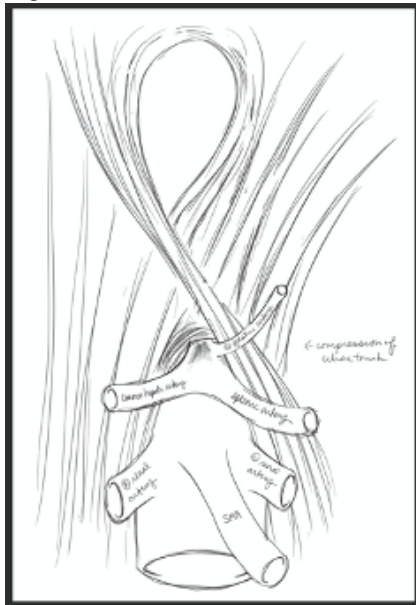
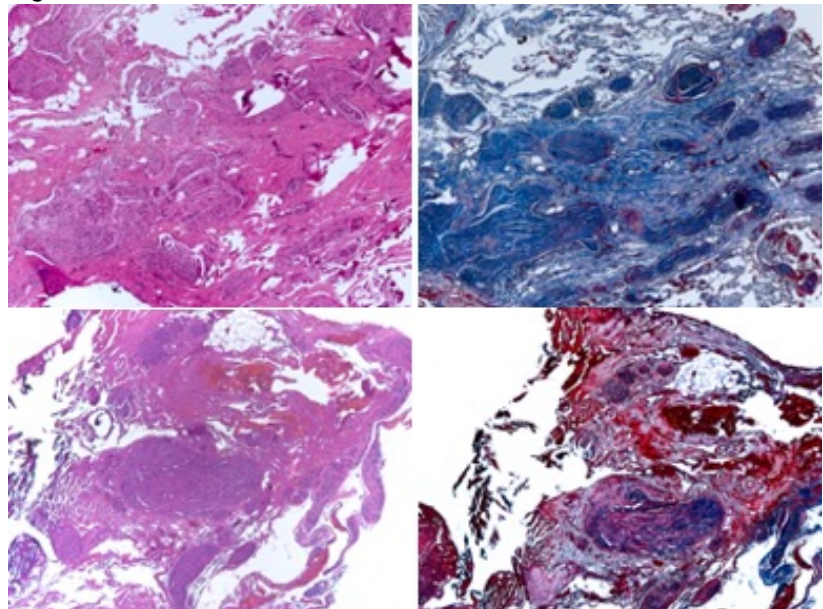


Figure 2 - 409



**Conclusions:** The clinico-pathologic findings seen in our patients and in literature support the hypothesis that the symptoms of MALS' patients are probably neurogenic. Although the presence of celiac artery narrowing is used as an important radiologic feature to diagnose MALS, only one of our patients showed severe vascular stenosis. The symptoms in this patient were relieved by nerve resection and without the need to perform vascular surgery. Our findings support the need to resect portions of the celiac plexus and/or perform intraoperative nerve blocks in individuals with severe symptoms that require surgical intervention.

**410 SMARCA4 (BRG1) Loss in Upper Gastrointestinal Adenocarcinoma is Not Exclusive to Tumors with Undifferentiated/Dedifferentiated/Rhabdoid Histology**

Matthew Gosse<sup>1</sup>, Robert Humble<sup>1</sup>, Ibrahim Abukhiran<sup>1</sup>, Andrew Bellizzi<sup>1</sup>

<sup>1</sup>University of Iowa Hospitals & Clinics, Iowa City, IA

**Disclosures:** Matthew Gosse: None; Robert Humble: None; Ibrahim Abukhiran: None; Andrew Bellizzi: None

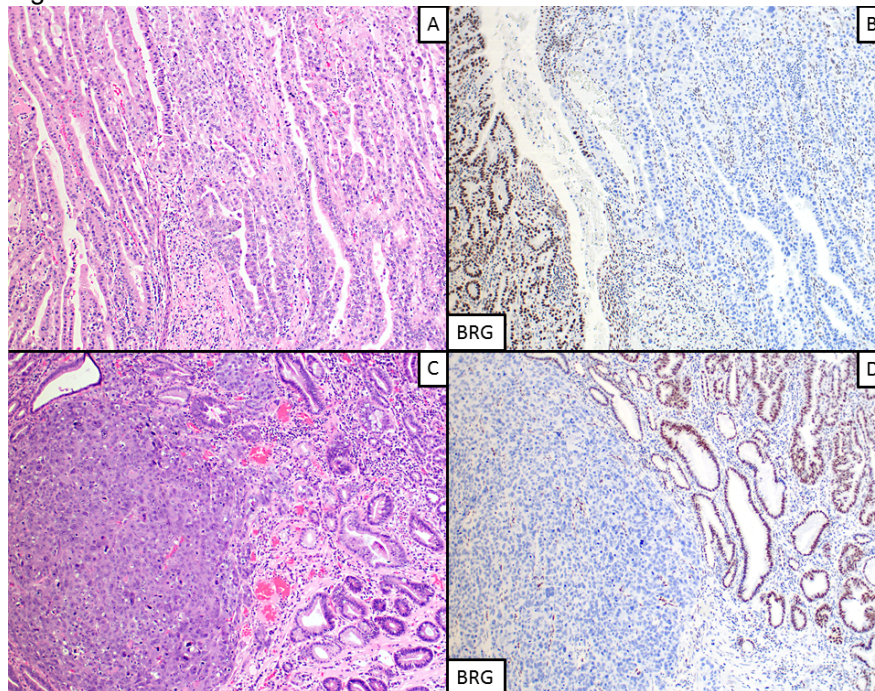
**Background:** Alterations in specific SWI/SNF complex subunits define some tumor types, including SMARCB1 (INI1) loss in pediatric malignant rhabdoid tumors and epithelioid sarcoma and SMARCA4 (BRG1) loss in small cell carcinoma of the ovary, hypercalcemic type. More recently, SWI/SNF subunit inactivation has been described in carcinomas with undifferentiated/dedifferentiated/rhabdoid morphology from diverse anatomic sites. Pan-cancer genomic studies have noted SWI/SNF subunit inactivation is uncommon but not rare, and we hypothesized that it would also be identified in some tumors with differentiated histology. Herein, we describe results of BRG1 immunohistochemistry (IHC) and clinicopathologic correlates in our institutional cohort of gastroesophageal and small intestinal adenocarcinomas.

**Design:** Tissue microarrays were constructed from all gastroesophageal (1991-2018) and small intestinal (1974-2018) adenocarcinomas with sufficient material to array. All original glass slides/pathology reports were reviewed for tumor epicenter (esophagus, GEJ, stomach, ampulla, duodenum, jejunum, and ileum), histologic subtype, and grade; age, gender, and overall survival were recorded, and BRG1 IHC was performed.

**Results:** We examined 404 specimens from 308 patients, including 93 esophageal, 75 GEJ, 66 gastric, 37 ampullary, 24 duodenal, 7 jejunal, and 5 ileal cancers. BRG1 loss was found in 2.2% of esophageal (n=2), 4.0% of gastroesophageal (n=3), and 1.5% of gastric (n=1) cancer patients (7 specimens from 6 patients overall). Loss was not observed in any small intestinal tumors. Loss was not significantly associated with histologic subtype, grade, stage, or overall survival (p>0.05). In the TMA, 4 cases showed discordant results between primary (intact) and lymph node metastasis (lost). In 2 cases, this was shown in whole section to correlate with subclonal BRG1 loss in

the primary tumor. BRG1 loss slightly predominated in tumors with differentiated (4 patients and 4 specimens) (Figure 1A-B), rather than dedifferentiated histology (2 patients and 3 specimens) (Figure 1C-D). BRG1 loss was not seen in mismatch repair deficient or Epstein-Barr virus (EBV)-positive tumors.

Figure 1 - 410



**Conclusions:** BRG1 loss was seen 3% of gastroesophageal adenocarcinomas and was not restricted to tumors with dedifferentiated histology. It was mutually exclusive of mismatch repair deficiency and EBV-positive status and was not demonstrably prognostically adverse.

#### **411 Extensive Evaluation of GATA-4 in 1479 Tumors Highlights Potential Diagnostic Applications as a Non-Colonic Pan-Gastrointestinal Marker**

Matthew Gosse<sup>1</sup>, Andrew Bellizzi<sup>1</sup>

<sup>1</sup>University of Iowa Hospitals & Clinics, Iowa City, IA

**Disclosures:** Matthew Gosse: None; Andrew Bellizzi: None

**Background:** SATB2 is widely utilized as a colon-specific gastrointestinal (GI) marker. We hypothesized that insights from developmental biology would lead us to a complementary non-colonic GI marker. While SATB2 is expressed in the developing intestine distal to the umbilicus, GATA-4 is expressed proximally. The GATA-4 knockout mouse demonstrates defects in tubal foregut, liver, and pancreatobiliary (PB) development. In a conditional GATA-4 knockout, jejunum is shifted to an ileal fate. We sought to extensively characterize GATA-4 immunohistochemical (IHC) expression in carcinomas and other epithelioid tumors.

**Design:** We optimized a GATA-4 mouse monoclonal antibody (clone 532020) for IHC and applied it to tissue microarrays of 1479 tumors, including 1407 epithelial neoplasms (mainly carcinomas) from diverse anatomic sites, 13 mesotheliomas, 14 melanomas, and 45 paragangliomas/pheochromocytomas. Staining was assessed for intensity (0-3+) and extent (0-100%) with an H-score calculated. Two tail Fisher's exact, Mann Whitney, and Kruskal-Wallis tests were performed with p<0.05 considered significant.

We also used cBioPortal to visualize GATA-4 mRNA expression in select TCGA tumor types.

**Results:** Detailed data are presented in the Table. GATA-4 was more frequently expressed by tubal gut tumors arising proximal to the umbilicus (i.e., proximal to ileum) (78% vs 14%,  $p < 0.0001$ ; median H-score 218 vs 70,  $p = 0.0001$ ), small intestinal vs colorectal (CRC) (70% vs 11%,  $p < 0.0001$ ; H-score 213 vs 70,  $p = 0.001$ ), combined upper GI (i.e., esophagus, GEJ, stomach, small intestine) and PB vs CRC (71% vs 11%,  $p < 0.0001$ ; H-score 165 vs 70,  $p = 0.003$ ), and upper GI vs PB carcinomas (78% vs 65%,  $p < 0.0001$ ; H-score 218 vs 117,  $p < 0.0001$ ). Among CRCs, positivity was more frequent on the right (19% vs 5%,  $p = 0.018$ ). Mucinous ovarian tumors were similarly highly expressing (68%; H-score 260), and expression did not vary between cystadenoma, borderline tumor, and carcinoma ( $p = 0.56$ ). GATA-4-positivity in neuroendocrine tumors was infrequent (8%), with all positive cases of pancreatic origin.

We observed high expression in non-neoplastic pancreatic acinar parenchyma and confirmed strong positivity (H-scores > 200) in whole sections of 3 acinar cell carcinomas.

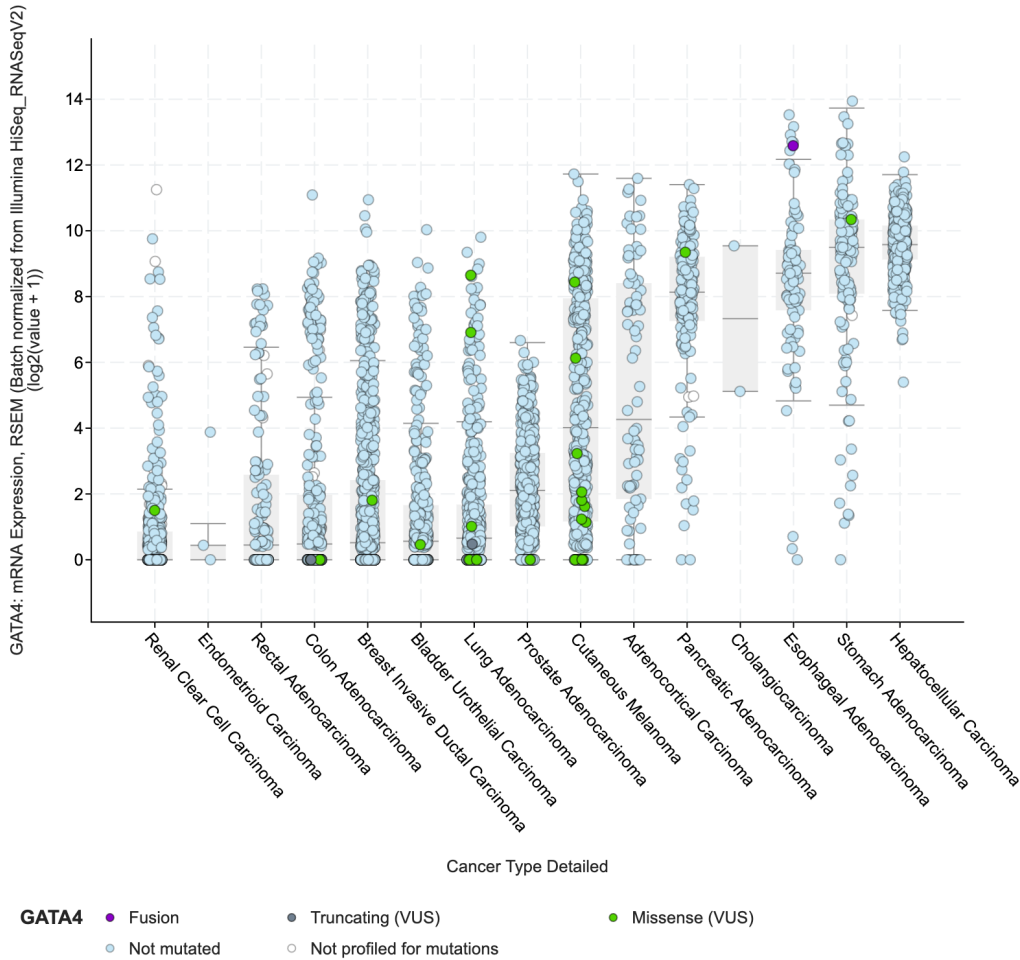
The visualized publicly available pan-cancer mRNA expression data are corroborative (Figure).

	Location	Positive (any H-score)	Total Number	Median H (if positive)	% H ≥ 50	% H ≥ 100	% H ≥ 200
GI Carcinoma	Stomach	89%	90	235	86%	81%	61%
	Esophagus	77%	129	225	68%	63%	46%
	Gastroesophageal Junction	76%	104	195	64%	56%	38%
	Small Bowel Foregut	73%	80	218	61%	56%	38%
	Pancreas	69%	273	105	51%	37%	11%
	Hepatocellular	61%	28	165	44%	37%	22%
	Cholangiocarcinoma	56%	134	142	40%	32%	19%
	Small Bowel Midgut	53%	15	213	33%	33%	33%
	Colon - Right	19%	68	70	12%	7%	3%
	Colon - Left	5%	75	68	4%	1%	0%
Other Carcinoma	Mucinous Ovarian	68%	100	260	65%	65%	49%
	Adrenal Cortical	11%	19	129	11%	5%	0%
	Non-Mucinous Mullerian	9%	53	33	2%	2%	2%
	NET	8%	48	180	8%	6%	4%
	Renal Cell Carcinoma	6%	33	23	0%	0%	0%
	Lung Adenocarcinoma	3%	29	37	0%	0%	0%
	Breast	2%	58	23	0%	0%	0%
	Thyroid	0%	43	N/A	N/A	N/A	N/A
Epithelioid Nonepithelial Neoplasm	Other (Prostate, SCC, Urothelial, NEC)	0%	15	N/A	N/A	N/A	N/A
	Mesothelioma	38%	13	147	23%	23%	15%
	Melanoma	29%	14	96	21%	14%	7%
	Pheochromocytoma	5%	22	88	5%	0%	0%
	Paraganglioma	0%	23	0	0%	0%	0%

H score is calculated by Strength (0,1+,2+,3+) x Extent (% positive cells)

GI = Gastrointestinal, NET = Neuroendocrine tumor, SCC = Squamous cell carcinoma, NEC = Neuroendocrine carcinoma

Figure 1 - 411



**Conclusions:** We have extensively evaluated the non-colonic pan-GI marker, GATA-4, highlighting several potential diagnostic applications, including 1. distinction of small intestinal from CRC (strong GATA-4-positivity favors the former, which have been shown to occasionally express SATB2 while CRC may be SATB2-negative), 2. distinction of upper GI from PB carcinomas (strong GATA-4-positivity favors the former), and 3. as a non-colonic pan-GI marker, especially useful in PB carcinomas (in which GATA-4-positivity [65%] outpaces CDX2 and CDH17 [30%]).

**412 Influence of Assay Conditions on Beta-Catenin Immunohistochemistry in Desmoid Fibromatosis: A Multi-Institutional Study**

Alexandra Isaacson<sup>1</sup>, Oyedele Adeyi<sup>2</sup>, Vijayalakshmi Ananthanarayanan<sup>3</sup>, Phyu Aung<sup>4</sup>, Mariza De Peralta-Venturina<sup>5</sup>, Raul Gonzalez<sup>6</sup>, Hans Magne Hamnvag<sup>3</sup>, Xiaoyin “Sara” Jiang<sup>7</sup>, Subramanya Sakaleshpura Mallikarjunappa<sup>8</sup>, Emily Meserve<sup>9</sup>, Dylan Miller<sup>10</sup>, Vinita Parkash<sup>11</sup>, Vijaya Reddy<sup>8</sup>, Anja Roden<sup>12</sup>, Francesca Ruggiero<sup>13</sup>, Lori Ryan<sup>14</sup>, Lauren Schwartz<sup>15</sup>, Jinru Shia<sup>16</sup>, Megan Troxell<sup>17</sup>, Justin Wells<sup>18</sup>, Yaping Wu<sup>19</sup>, Andrew Bellizzi<sup>1</sup>

<sup>1</sup>University of Iowa Hospitals & Clinics, Iowa City, IA, <sup>2</sup>University of Minnesota Medical School, Minneapolis, MN, <sup>3</sup>Loyola University Medical Center, Maywood, IL, <sup>4</sup>The University of Texas MD Anderson Cancer Center, Houston, TX, <sup>5</sup>Cedars-Sinai Medical Center, Los Angeles, CA, <sup>6</sup>Beth Israel Deaconess Medical Center, Harvard Medical School, Boston, MA, <sup>7</sup>Duke University, Durham, NC, <sup>8</sup>Rush University Medical Center, Chicago, IL, <sup>9</sup>Spectrum Healthcare Partners, South Portland, ME, <sup>10</sup>Intermountain Central Laboratory, Salt Lake City, UT, <sup>11</sup>Yale School of Medicine, Yale School of Public Health, New Haven, CT, <sup>12</sup>Mayo Clinic, Rochester, MN, <sup>13</sup>Penn State Health Milton S. Hershey Medical Center, Hershey, PA, <sup>14</sup>Allina Health Laboratories, Plymouth, MN, <sup>15</sup>Perelman School of Medicine at the University of Pennsylvania, Philadelphia, PA, <sup>16</sup>Memorial Sloan Kettering Cancer Center, New York, NY, <sup>17</sup>Stanford University Medical Center, Stanford, CA, <sup>18</sup>Walter Reed National Military Medical Center, Rockville, MD, <sup>19</sup>Providence Health and Services, Portland, OR

**Disclosures:** Alexandra Isaacson: None; Oyedele Adeyi: None; Vijayalakshmi Ananthanarayanan: None; Phyu Aung: None; Mariza De Peralta-Venturina: None; Raul Gonzalez: None; Hans Magne Hamnvag: None; Xiaoyin “Sara” Jiang: None; Subramanya Sakaleshpura Mallikarjunappa: None; Emily Meserve: None; Dylan Miller: None; Vinita Parkash: None; Vijaya Reddy: None; Anja Roden: None; Francesca Ruggiero: None; Lauren Schwartz: None; Jinru Shia: None; Megan Troxell: None; Justin Wells: None; Yaping Wu: None; Andrew Bellizzi: None

**Background:** Immunohistochemical (IHC) assays should be developed, optimized, and validated for a specific clinical purpose (i.e., “fit-for-purpose”). An assay is ultimately judged on its ability to perform in specific diagnostic contexts. Desmoid fibromatosis is a locally aggressive deep soft tissue tumor of fibroblastic lineage driven by mutations in *CTNNB1* or *APC*, leading to nuclear beta-catenin accumulation. Nuclear beta-catenin staining is reported to be sensitive and specific for the diagnosis of desmoid. Recent discussion among clinical IHC laboratory directors revealed significant variability in director and ordering pathologist satisfaction with beta-catenin performance in this setting. We hypothesized that differences in laboratory assay conditions would underlie the varied performance. We were also interested to correlate staining between tissue microarrays (TMAs) and corresponding whole sections to determine if TMAs are a reasonable option for future “crowdsourced” IHC assay comparison studies.

**Design:** Unstained slides from TMAs of 15 desmoids and 15 leiomyosarcomas (arrayed in duplicate, 1.5 mm cores) and whole sections (WS) of 2 of the desmoids in the TMA were sent to 18 clinical laboratories. Beta-catenin IHC was performed under each laboratory’s normal conditions. Nuclear staining for beta-catenin was scored from 0-4 (1=1-25%, 2=26-50%, 3=51-75%, 4=76-100%) with results for duplicate cores averaged. Laboratories also submitted their assay conditions, including clone, staining platform, antigen retrieval solution and pH, and detection chemistry. Sensitivity and specificity were calculated for each laboratory’s assay and for the entire cohort. Mean WS and corresponding TMA scores were calculated. Mann-Whitney and Kruskal-Wallis tests with post tests were used with  $p < 0.05$  considered significant.

**Results:** The mean sensitivity and specificity for nuclear beta-catenin positivity in desmoid fibromatosis was 84% and 91%. The ranges of sensitivity and specificity for individual assays were 31%-100% and 40%-100%. The frequencies of various assay conditions are listed in the Table. Median sensitivity and specificity varied significantly between staining platforms ( $p=0.02$ ,  $p=0.04$ ) and approached significance for clone (specificity) and detection chemistry. WS had a higher mean score than corresponding tumors in the TMA (2.6 vs. 1.6,  $p=0.0018$ ).

Variable	Number of Laboratories (n=18)	Median Sensitivity		Median Specificity	
<b>CLONE</b>					
14	13	82%		100%	
17C2	3	100%	p=0.13	87%	p=0.06
Beta-Catenin-1	2	66%		90%	
<b>PLATFORM</b>					
Ventana Benchmark Ultra	10	85%		100%	
Leica Bond III	6	100%	p=0.02	84%	p=0.04
Dako Autostainer Link 48	2	45%		100%	
<b>ANTIGEN RETRIEVAL SOLUTION</b>					
Ventana CC1	10	85%		100%	
Leica ER1	3	100%		80%	
Leica ER2	3	100%	p=0.08	87%	p=0.17
Dako TRS, pH 6	1	59%		100%	
Dako TRS, pH 9	1	31%		100%	
<b>ANTIGEN RETRIEVAL pH</b>					
Low	4	81%		90%	
High	14	91%	p=0.79	97%	p=0.52
<b>DETECTION CHEMISTRY</b>					
Bond Polymer Refine	6	100%		84%	
Ventana UltraView	6	79%		97%	
Ventana OptiView	3	94%	p=0.06	100%	p=0.09
Dako EnVision	2	45%		100%	
Ventana iView	1	76%		93%	

**Conclusions:** Beta-catenin assay conditions vary widely among laboratories, and staining platform may contribute to differences in sensitivity and specificity of nuclear staining for the diagnosis of desmoid fibromatosis. TMAs are highly useful for crowdsourcing assay comparisons, although WS may provide more accurate information on extent of staining in paucicellular tumors.

**413 Monitoring Intraoperative Frozen Sections from 2016-2020 Using a Standardized Classification Model: An Institutional Experience**

Meena Kashi<sup>1</sup>, Joel Lanceta<sup>1</sup>, Kingsley Ebare<sup>2</sup>, Anupma Agarwal<sup>1</sup>, Mesut Toprak<sup>1</sup>, Lynne M Opitz<sup>1</sup>  
<sup>1</sup>Staten Island University Hospital/Northwell Health, Staten Island, NY, <sup>2</sup>Staten Island University Hospital/Northwell Health, Baylor College of Medicine, TX

**Disclosures:** Meena Kashi: None; Joel Lanceta: None; Kingsley Ebare: None; Anupma Agarwal: None; Mesut Toprak: None

**Background:** The frozen section (FS) procedure is an important responsibility to provide a rapid and accurate intraoperative diagnosis. It comes with many limitations, including sampling errors, freezing artifacts, and lack of special studies. The College of American Pathologists (CAP) has recommended the following institutional FS quality benchmarks: a deferral rate ≤ 4%, a turnaround time of ≤ 20 minutes for 90% of cases, and a concordance rate between FS diagnosis and permanent section to be between 92-98%. Large institutions implemented standardized classification models to compare their FS statistics to the CAP benchmarks. Few reports have focused on how medium to small-sized community hospitals can use these models to monitor their FS quality standards.

**Design:** A retrospective review of all intraoperative frozen consultations (n = 2530) at our hospital from 1/1/2016 to 5/7/2020 was performed by five pathology residents. Data collected on each consultation included age, gender, tissue type, turnaround time, FS diagnosis and final diagnosis. The final pathology diagnosis was compared with the FS diagnosis and classified by concordance: concordant (FS diagnosis and final diagnosis are similar), discrepant (FS diagnosis and final diagnosis are different), or deferred (indeterminant diagnosis at the time of FS examination). Statistical analysis for concordance was performed using SAS 9.4.

**Results:** 2530 FS cases were reviewed from 1522 patients. The mean age of the patient was 60.5 (range 1.5 to 93), and by gender, F:M was 3:1. 66.3% of cases (n=1678) had a turnaround time ≤ 20 minutes (Figure 1). 91.58% (n=2317) of the FS cases were concordant, 3.4% were discrepant (n = 86) and 5.0% were deferred (n = 127). Most discrepant cases were attributed to histologic sampling error (n = 57, 76%) from sentinel nodes of the breast, with interpretation errors accounting for 24% of discrepancies (n=21) (Figure 2). The majority of deferred FS specimen

were from the female genital system (n=27), followed by head and neck (n = 25) and central nervous system (n = 23).

Figure 1 - 413

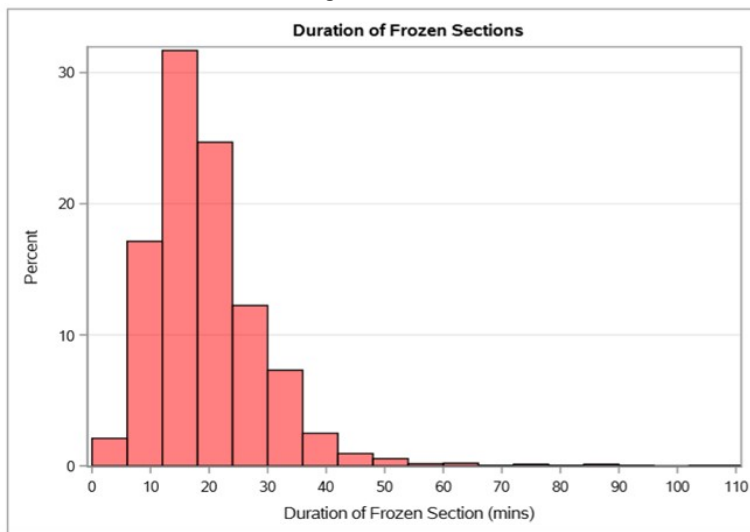
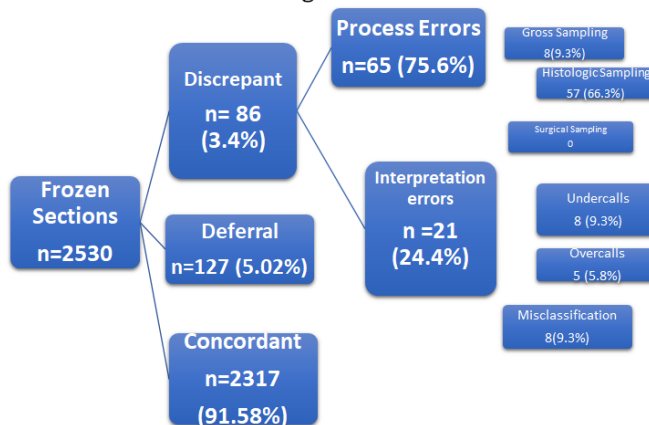


Figure 2 - 413

Classification of Frozen Sections by Concordance with Final Diagnosis



**Conclusions:** This study shows that a standardized model is useful to identify gaps in FS benchmarks in a community hospital. We identified turnaround time as not meeting the CAP benchmark and implemented improvements, including a designated FS microscope, required clinical information on voucher in complicated specimens, and increased readiness of staff and technicians. We are proceeding with an annual review of FS specimens and monthly QAs sessions to track agreement and determine where systemic or individual improvements can be made.

**414 CD31 Expression in Benign and Neoplastic Hematolymphoid Lesions**

Mahyar Khazaeli<sup>1</sup>, Mehran Taherian<sup>1</sup>, Mihai Merzianu<sup>2</sup>

<sup>1</sup>University at Buffalo, SUNY, Buffalo, NY, <sup>2</sup>Roswell Park Comprehensive Cancer Center, Buffalo, NY

**Disclosures:** Mahyar Khazaeli: None; Mehran Taherian: None; Mihai Merzianu: None



**Background:** CD31 (platelet endothelial cell adhesion molecule-1 [PECAM-1]), the ligand for CD38, is a pan-endothelial marker also expressed on the surface of circulating platelets, neutrophils, monocytes, and leukocytes. CD31 is widely used in clinical diagnosis for lineage determination and in research for vascular lumina quantification. CD31 is also expressed in plasma cells and plasmablastic neoplasms as well as histiocytes which may create differential diagnostic challenges with vascular neoplasms. CD31 expression in benign and neoplastic hematolymphoid cells is less studied and is assessed here in various hematolymphoid lesions.

**Design:** A tissue microarray was constructed with paraffin-embedded tissue samples obtained from 84 specimens using a Manual Tissue Microarrayer (MTA-1, Beecher Instruments, Sun Prairie, WI). On average, 2 cores were harvested (range, 1-4 cores) from each lesion sampled at least in duplicate when possible. A total of 260 cores (0.6-mm diameter) were obtained. CD31 staining (1:25, DAKO clone JC70A, Carpinteria, CA) was performed on the TMA and 46 full sections. In total, 126 lesions were included, 27 benign and 99 neoplastic, from nodal (n=59), splenic (n=14), bone marrow (n=18), and extranodal (n=35) sites. Mature B cell neoplasms (n=57) were mostly low grade (n=39), but mature T cell (n=12), plasma cell (n=4), lympho- or myeloblastic tumors (n=16), and Hodgkin lymphoma (n=10) were also included. Benign nodal, splenic, thymic, or extranodal lesions comprised follicular hyperplasia, paracortical expansion, and plasmacytosis. H score (0- 8.0) derived from percentage (0: 0-4%, 1: 5-20%, 2: 21-40%, 3: 41-60%, 4: 61-80%, 5: 81-100%) and intensity (0 no staining, 1+ weak, 2+ moderate, 3+ strong) sum was considered positive when H >=3. Only membranous labeling was quantified. Cases with a negative reaction in endothelial cells and megakaryocytes or with missing cores were excluded.

**Results:** Overall, CD31 was positive in 68/126 (54%) of the tested lesions with the highest expression in hairy cell leukemia (H=8.0) and plasma cell neoplasms (H=7.0). H score was 3.6 in acute leukemia blasts and 4.2 in Reed Sternberg cells. B cell lymphomas had a higher CD31 expression than T cell lymphomas (H, 3.5 vs 2.5), and low-grade B cell neoplasms had a significantly higher expression than high-grade B cell tumors (H, 4.4 vs 0.9, p=0.01). CD31 expression was higher in reactive follicular hyperplasia compared to follicular lymphoma (H, 2.9 vs 1.4). In contrast, benign mantle zone cells showed a lower expression than mantle cell lymphoma (H, 2.3 vs 5).

**Conclusions:** CD31 is commonly expressed in a variety of benign and neoplastic, B and T cell proliferations in addition to plasma cells and histiocytes. Awareness of this finding is relevant for the diagnostic and research applications of this marker.

#### **415 Histopathologic Findings in Hernia Sac: A Clinical and Pathological Review**

Natalia Lashmanova<sup>1</sup>, Matthew Vega<sup>1</sup>, Vijaya Reddy<sup>1</sup>, Paolo Gattuso<sup>1</sup>, Lin Cheng<sup>1</sup>

<sup>1</sup>Rush University Medical Center, Chicago, IL

**Disclosures:** Natalia Lashmanova: None; Matthew Vega: None; Vijaya Reddy: None; Paolo Gattuso: None; Lin Cheng: None

**Background:** Routine histopathologic examination of hernia sac in adults remains a controversial topic among general surgical pathologists. We undertook a retrospective study to assess possible clinical benefits from pathological examination of hernia sac specimens.

**Design:** Our pathology database between 1992 and 2020 was searched for adult specimens submitted as hernia sac. The clinical and pathological data of patients with abnormal histopathologic findings were reviewed.

**Results:** There were a total of 5424 hernia sac surgical specimens, including 3722 inguinal (right 1831 and left 1891), 1625 umbilical and 77 femoral. A total of 44/5424 (0.8%) cases revealed abnormal histopathologic findings (32 malignant and 12 benign). 32/5424 (0.5%) were malignant tumors (28 epithelial and 4 lymphoid). 25 cases were located in the umbilical region (20 female and 5 male, age range 36 - 89 with a mean of 67). 12/25 (48%) cases presented as primary clinical manifestations of the disease (5 gastrointestinal tract carcinomas, 5 gynecological tract carcinomas and 2 lymphoid neoplasms). 13/25 (52%) cases were relapses/recurrences of the tumors (8 gynecological carcinomas, 3 colon carcinomas, 1 breast carcinoma, and 1 lymphoma). Among the 7 malignant inguinal hernia cases (4 male and 3 female, age range 70-85 with a mean of 75), 3 were primary presentation of the tumor (2 prostatic carcinoma, 1 pancreatic carcinoma), and 4 were metastases (2 ovarian carcinoma, 1 colon carcinoma, 1 lymphoid). 12/44 (27%) cases were benign lesions. 7/12 cases were adrenal rest located in the inguinal region. All 7 patients were male with age range 27-87 and a mean of 58. The remaining 5

cases included 4 cases of endometriosis (3 umbilical and 1 inguinal, mean age of 45) and 1 case of inguinal sarcoidosis.

**Conclusions:** The incidence of malignancy in hernia sacs was 32/5424 (0.5%). The most common malignancy encountered was from nearby organs: gynecological and gastrointestinal tracts. However distant metastases from breast and prostate were also seen. 15/32 (47%) malignant cases presented as the first clinical manifestation. Most malignant cases 23/32 (72%) were from female.

The most common benign lesion encountered was adrenal rest.

In summary, routine histopathologic examination of hernia sac in adults is recommended, since it may provide important clinical information aiding patient management.

#### **416 Morphological Assessment of Kidney and Smooth Muscle Tumors Sent for Fumarate Hydratase Immunohistochemistry: A Reference Laboratory Experience**

Valarie McMurtry<sup>1</sup>, Jonathon Mahlow<sup>2</sup>, Elke Jarboe<sup>2</sup>, Lesley Lomo<sup>3</sup>, Deepika Sirohi<sup>1</sup>

<sup>1</sup>The University of Utah, Salt Lake City, UT, <sup>2</sup>The University of Utah/ARUP Laboratories, Salt Lake City, UT, <sup>3</sup>University of Utah Health Sciences Center/Huntsman Cancer Institute, Salt Lake City

**Disclosures:** Valarie McMurtry: None; Jonathon Mahlow: None; Elke Jarboe: None; Lesley Lomo: None; Deepika Sirohi: None

**Background:** Fumarate hydratase (FH) deficient tumors can occur due to germline mutations in hereditary leiomyomatosis with renal cell carcinoma syndrome (HLRCC) or somatic mutations. Identification of FH-deficient tumors is critical to screen patients for germline mutations. FH-deficient tumors have distinct morphology on H&E, and FH immunohistochemistry (IHC) is commonly used to confirm FH-deficient tumors. In this study, we aim to refine the morphologic criteria by reviewing specimens deemed to meet published morphologic criteria by the referring pathologist and sent to a reference laboratory for IHC staining.

**Design:** Tumor specimens that were sent for FH IHC testing from 10/2019 to 7/2020 were collected. H&E stained slides were reviewed: smooth muscle tumors (SMTs) and kidney tumors were reviewed by 2 gynecologic and 2 genitourinary pathologists respectively. HLRCC-like nuclei are defined as melanoma-like nucleoli with halos. Consensus was reached on discordant assessments. Fisher's exact test was used for analysis.

**Results:** 22 Kidney tumors (5 FH-deficient) and 51 SMTs (27 FH-deficient) were reviewed. FH-deficient SMTs were significantly more likely to have staghorn vessels, eosinophilic cytoplasmic inclusions, schwannoma-like areas, or HLRCC-like nuclei ( $p < 0.05$  for each). Edema and nuclei arranged in cords showed no association. In Kidney tumors, a cord like growth pattern, rhabdoid change, absence of coagulative tumor necrosis, and psammoma bodies were exclusively seen in FH deficient tumors. They were more likely to show nested growth and sieve-like architecture (3/5 vs 3/17 for both patterns), and less likely to be papillary (1/5 vs 12/17), though not statistically significant. Other features evaluated: nuclear grade, in situ dysplasia, HLRCC-like nuclei, reticular growth, intracystic growth, solid sheets, tubular architecture, and infiltrating glands overlapped across both groups.

**Conclusions:** Identification of FH-deficient tumors by morphology is difficult as the described characteristics overlap with many FH-intact tumors. However, FH-deficient SMTs submitted for FH IHC testing were significantly more likely to show staghorn vessels, eosinophilic cytoplasmic inclusions, schwannoma-like areas, or HLRCC-like nuclei. While varied morphologies and HLRCC-like nuclei have been previously described in kidney tumors and were interrogated in this limited study – we have found that the presence of cord or sieve-like architecture may be a yet underappreciated feature that could better identify these lesions for further workup.

**417 Clinical Utility of NGS-Based Gene Fusion Testing in Solid Tumors**

Behtash Nezami<sup>1</sup>, Gokce Toruner<sup>1</sup>, Mark Routbort<sup>1</sup>, Francis San Lucas<sup>1</sup>, Richard Yang<sup>1</sup>, Rana Seyedjafari<sup>1</sup>, Hui Chen<sup>1</sup>, Asif Rashid<sup>1</sup>, Sanam Loghavi<sup>1</sup>, Sinchita Roy-Chowdhuri<sup>1</sup>, Rashmi Kanagal-Shamanna<sup>1</sup>, C. Cameron Yin<sup>1</sup>, Zhuang Zuo<sup>1</sup>, Chi Young Ok<sup>1</sup>, Zhenya Tang<sup>1</sup>, L. Jeffrey Medeiros<sup>1</sup>, Rajyalakshmi Luthra<sup>1</sup>, Keyur Patel<sup>1</sup>

<sup>1</sup>The University of Texas MD Anderson Cancer Center, Houston, TX

**Disclosures:** Behtash Nezami: None; Gokce Toruner: None; Mark Routbort: None; Francis San Lucas: None; Richard Yang: None; Rana Seyedjafari: None; Hui Chen: None; Asif Rashid: None; Sanam Loghavi: None; Sinchita Roy-Chowdhuri: None; Rashmi Kanagal-Shamanna: None; C. Cameron Yin: None; Zhuang Zuo: None; Chi Young Ok: None; Zhenya Tang: None; L. Jeffrey Medeiros: None; Rajyalakshmi Luthra: None; Keyur Patel: None

**Background:** Gene fusions provide clinically actionable diagnostic, prognostic and therapeutic information in oncology. Next-generation sequencing (NGS)-based multi-gene fusion testing of RNA from solid tumor tissues allows systematic screening for clinically actionable gene fusions. Here, we report the clinical experience with >5,000 clinical solid tumor samples tested using a NGS-based 51-gene fusion assay.

**Design:** RNA extracted from formalin-fixed, paraffin embedded (FFPE) tissue specimens and cytology specimens were analyzed for gene fusions in 51 genes using an amplicon-based NGS assay on a semiconductor-based sequencing platform. A total of 5,236 clinical cases were tested for inter- and intragenic fusions involving *AKT2*, *ALK*, *AR*, *AXL*, *BRAF*, *BRCA1*, *BRCA2*, *CDKN2A*, *EGFR*, *ERBB4*, *ERBB2*, *ERG*, *ESR1*, *ETV1*, *ETV4*, *ETV5*, *FGFR1*, *FGFR2*, *FGFR3*, *FGR*, *FLT3*, *JAK2*, *KRAS*, *MDM4*, *MET*, *MYB*, *MYBL1*, *NF1*, *NOTCH1*, *NOTCH4*, *NRG1*, *NTRK1*, *NTRK2*, *NTRK3*, *NUTM1*, *PDGFRA*, *PDGFRB*, *PIK3CA*, *PPARG*, *PRKACA*, *PRKACB*, *PTEN*, *RAD51B*, *RAF1*, *RB1*, *RELA*, *RET*, *ROS1*, *RSPO2*, *RSPO3*, and *TERT*.

**Results:** The analysis was successful in 4,599 of 5,236 (87.8%) clinical samples tested, of which 343 (7.5%) were positive and 4,256 (92.5%) were negative for a gene fusion. No results could be obtained due to suboptimal quantity or quality of RNA in 637 (12.2%) samples. Detailed clinicopathologic annotations are available for 2,353 samples. Non-small cell lung carcinoma (NSCLC, n=627, 26.6%), colorectal adenocarcinoma (n=452, 19.2%), and glioblastoma (n=183, 7.8%) were the top 3 tumor types tested (Figure 1). The top two fusions detected across all cancer types were *EML4-ALK* (n=43), exclusively detected in lung cancers, and *MET* exon 14 skipping (n=23), detected in lung cancers, glioblastoma and colorectal adenocarcinoma (Figure 2). Within each specific tumor type, the highest rates of fusion were detected in prostatic adenocarcinoma (*TMPRSS2-ERG*; 13/20, 65%) followed by adenoid cystic carcinoma (*NFIB*; 5/8, 62.5%), papillary thyroid carcinoma (31/173, 17.9%), and NSCLC (*ALK*, *BRAF*, *RET*, *ROS1*, *NRG1*, 83/627, 13.2%). Unsuspected fusions with direct impact on diagnosis and clinical management were detected on a regular basis throughout the testing period. Significantly, targetable fusions with available approved therapy were detected in 127/2,353 (5.4%) cases, including 79/627 (12.6%) in NSCLC, 34/274 (12.4%) in thyroid carcinomas, and 7/173 (4%) squamous lung carcinoma were targetable (Figure 1).

Figure 1 - 417

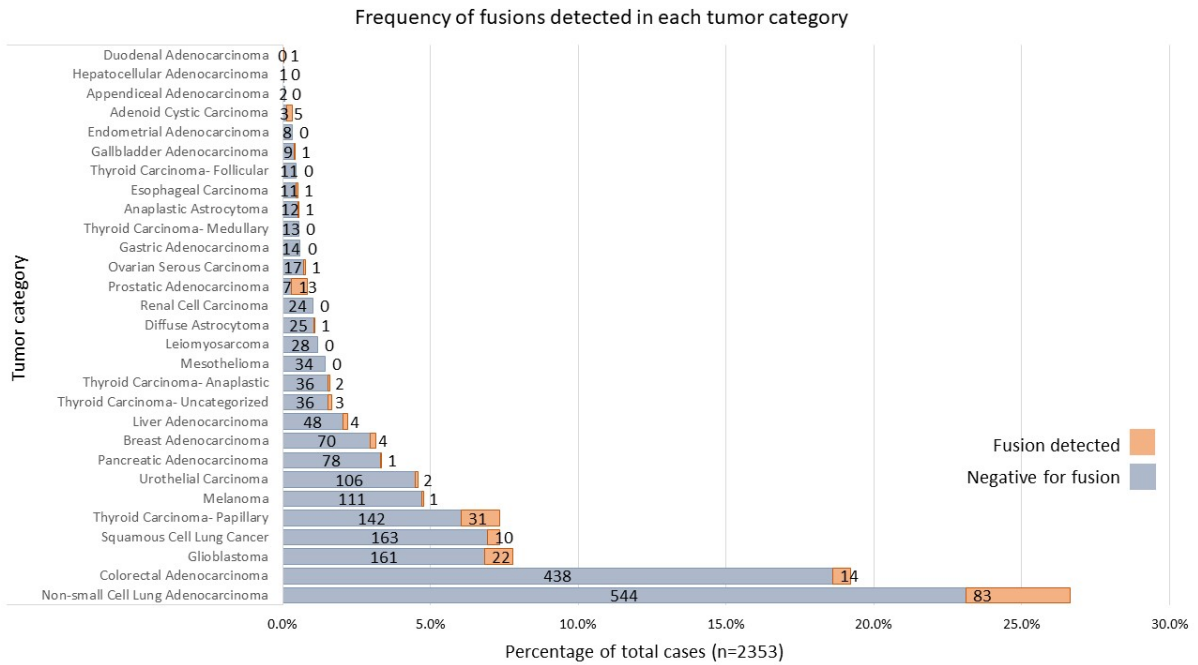
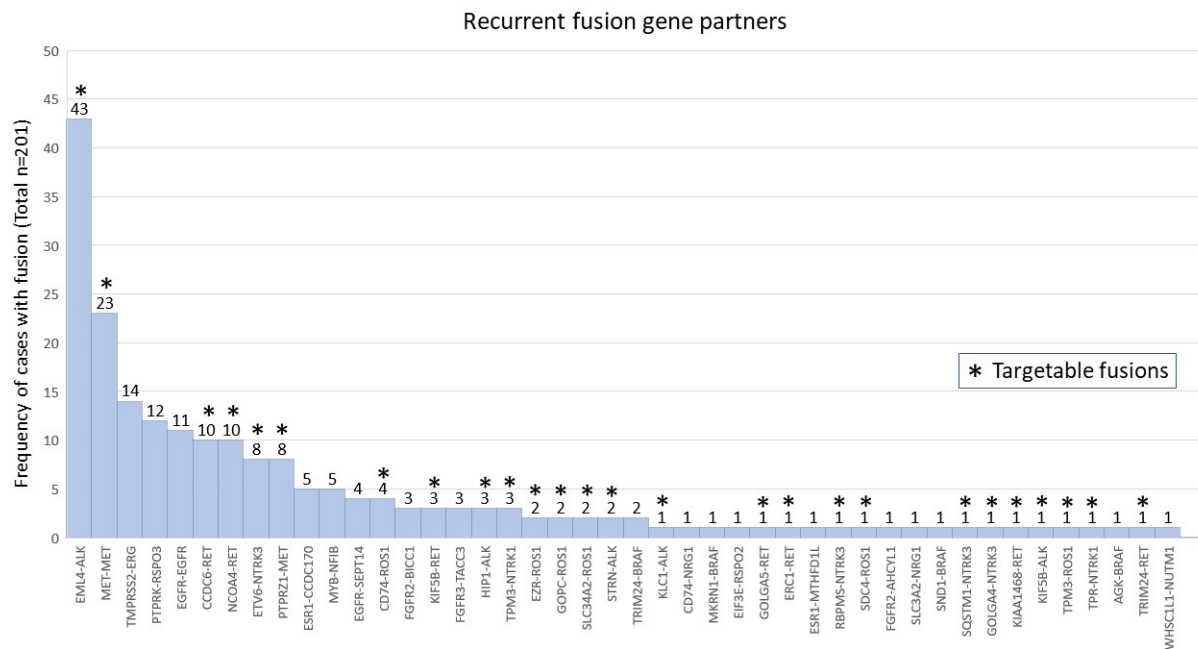


Figure 2 - 417



**Conclusions:** This large clinical cohort shows a high success rate for NGS-based fusion testing of solid tumor specimens, and also identified clinically actionable gene fusions across a range of tumor types. These data prove the feasibility and provide justification for incorporating panel-based fusion testing in standard-of-care clinical testing. The lessons learned are also valuable for improving the success rate of clinical RNA-based fusion testing for solid tumors.

**418 Biomarker Expression in SMARCA4-Deficient Tumors Suggests Potential Therapeutic Targets**

Lacey Schrader<sup>1</sup>, Jennifer Boland Froemming<sup>1</sup>, Sarah Jenkins<sup>1</sup>, Rondell Graham<sup>1</sup>, Grant Spears<sup>1</sup>, Julie Vrana<sup>1</sup>, Anja Roden<sup>1</sup>, Aaron Mansfield<sup>1</sup>  
<sup>1</sup>Mayo Clinic, Rochester, MN

**Disclosures:** Lacey Schrader: None; Jennifer Boland Froemming: None; Sarah Jenkins: None; Rondell Graham: None; Grant Spears: None; Julie Vrana: None; Anja Roden: None; Aaron Mansfield: *Consultant*, Bristol-Myers Squibb, Abbvie, Genentech/Roche, Astra Zeneca

**Background:** SMARCA4-deficient tumors are aggressive neoplasms characterized by mutation of the SMARCA4 gene, a subunit of the ATP-dependent SWI/SNF chromatin remodeling complex encoding Brahma-related gene-1 (BRG1). Outcome of these tumors is dismal and no specific treatment is available. However, clinical trials using EZH2 inhibitors are underway. We aim to evaluate the expression and prognostic role of biomarkers including PD-L1, EZH2, and NTRK in patients with SMARCA4-deficient tumors.

**Design:** Resected or biopsied SMARCA4-deficient tumors (1996-2020) were retrospectively identified by confirming loss of BRG1-expression by immunohistochemistry (IHC). Clinical information was collected from medical records. EZH2 (clone D2C9), PD-L1 (22C3), and pan-TRK (EPR17341) expression was assessed independently by 2 observers. Expression was recorded as percent (%) and intensity of tumor cell nuclei staining (EZH2), % of membranous/cytoplasmic tumor cell staining (pan-TRK), or % of membranous tumor (tumor proportion score, TPS) and tumor-infiltrating lymphocytes (TILs) staining (PD-L1). Statistical analysis was performed.

**Results:** Thirty-eight SMARCA4-deficient tumors (24 men, 63.2%; median age, 59 years, range, 32-81) included 27 thoracic, 8 extra-thoracic, and 3 tumors of unclear primary site. Twenty-four (of 26, 92.3%) patients were smokers. Thirty (of 36, 83.3%) had metastases at time of diagnosis. Seven (of 38, 18.4%) underwent complete resection; 17 (of 18, 94.4%) patients received neoadjuvant and/or adjuvant therapy. Results of IHC are summarized in table 1. In a median follow up time of 3.6 months (range, 12 days-23.7 months) (N=17) 12 patients died of disease (range 12 days to 22 months) and 5 were alive with disease. PD-L1 TPS or TILs and Pan-TRK expression were not associated with overall survival.

Feature	Results
Interobserver Variability	Weighted Kappa
EZH2 (<50%; ≥50%)	1.00
PD-L1 TPS <sup>a</sup> (<1%; 1-49%; ≥50%)	0.94
PD-L1 TILs <sup>b</sup> (<1%; ≥1%)	0.85
NTRK (<1%; ≥1%)	0.93
Expression of IHC markers in tumors	
EZH2	35
N	99.3 (90-100)
Median % EZH2-positive tumor cells, range	35 (100)
Strong intensity of expression, N (%)	
PD-L1 TPS <sup>a</sup>	38
N	15 (39.5)
<1%, N (%)	13 (34.2)
1-49%	10 (26.3)
≥50%	
PD-L1 TILs <sup>b</sup>	33
N	7 (21.2)
<1%, N (%)	14 (42.4)
1-24%	2 (6.1)
25-49%	10 (30.3)
≥50%	
Pan-TRK	36
N	26 (72.2)
<1%, N (%)	5 (13.9)
1-5%	3 (8.3)
6-49%	2 (5.6)

≥50%
<sup>a</sup> Tumor proportion score
<sup>b</sup> Tumor-infiltrating lymphocytes

**Conclusions:** Given the uniform high expression of EZH2, PD-L1 expression in ≥1% of tumor cells in more than 50% of cases, and pan-TRK expression in ≥1% of tumor cells in more than a quarter of cases together with the almost perfect reproducibility of biomarker expression in our series, targeted therapy might be a treatment option in a substantial proportion of patients with SMARCA4-deficient tumors. More follow up data are necessary to evaluate for the possible predictive value of these biomarkers.

**419 Mass Forming Immunoglobulin G4-Related Disease: A Potential Distinct Subtype, Clinicopathological Analysis of A Series of 15 Cases**

Ruoyu Shi<sup>1</sup>, Kenneth Chang<sup>2</sup>, Angela Takano<sup>1</sup>, Joe Yeong<sup>1</sup>, Benjamin Farah<sup>3</sup>, Kuick Hong<sup>4</sup>  
<sup>1</sup>Singapore General Hospital, Singapore, Singapore, <sup>2</sup>KKH, Singapore, <sup>3</sup>Singapore, Singapore, <sup>4</sup>KK Women's and Children's Hospital, Singapore

**Disclosures:** Ruoyu Shi: None; Kenneth Chang: None; Angela Takano: None; Joe Yeong: None; Benjamin Farah: None; Kuick Hong: None

**Background:** The purpose of this study is to characterize the clinicopathological features of mass forming Immunoglobulin G4-related disease (IgG4-RD).

**Design:** A retrospective search for cases of mass forming IgG4-RD diagnosed at Singapore General Hospital between 2008 and 2019 was performed. We analyzed the clinicopathological characteristics of these patients.

**Results:** We found a total of 15 cases of mass forming IgG4-RD. The male to female ratio was 2.5:1 and the median age was 61 years old. The majority of cases showed a solitary lesion (12/15) with a median size of 46mm. IgG4-RD was considered as a clinical differential diagnosis only in one case (1/15) prior to the radical operation. Diagnostic histopathological features such as dense lymphoplasmacytic infiltration positive for IgG4 plasma cells (15/15), storiform fibrosis (15/15), and obliterative phlebitis (9/15), were observed in most cases. These findings were distributed heterogeneously within the lesions. Cases with single organ involvement showed a low relapse rate (2/10) and normal serum IgG4 level after radical resection.

**Table 1. Key clinical and Pathological Features of Mass Forming IgG4-RD**

Case	Age <sup>c</sup> (y)	Organ	Lesion number	Lesion size (mm)	Histology <sup>d</sup>	IgG4 count <sup>e</sup>	IgG4/IgG ratio <sup>e</sup>	Post-op IgG4 serum level <sup>g</sup>	Systemic Disease	Followup(m)	Relapse
1	43	Submandibular gland	1	21	1,2	110	0.84	No	Likely <sup>i</sup>	168	Yes <sup>i</sup>
2	74	Pancreas	1	40	1,2,3	134	0.91	No	No	120	Yes <sup>j</sup>
3	55	Submandibular gland	1	25	1,2	254	0.88	0.42	Possible <sup>k</sup>	84	Yes <sup>k</sup>
4	77	Liver	1	39	1,2,3.	62	0.63	No	No	78	No
5	53	Small bowel	1	55	1,2	108	0.78	No	No	12	No
6	62	Large bowel	1	50	1,2	105	0.81	1.37	No	60	No
7	50	Liver	1	25	1, 2,3	35	0.33	0.51	No	54	No
8	71	Lung	1	20	1, 2,3	113	0.66	>3.4	Yes	36	No
9	72	Lung	5	129	1, 2,3	55	0.4	1.28	No	48	No
10	72	Submandibular glands	4	25	1,2.	207	0.67	No	No	36	No
11	43	Kidney	1	40	1,2,3	98	0.77	No	No	120	Yes <sup>a</sup>
12 <sup>a</sup>	53	Lung	2	35	1,2,3	100	0.5	0.61	No	18	No
13	62	Large bowel	1	75	1,2,3	360	0.84	0.35	No	20	No
14	78	Small bowel	1	65	1,2,3	118	0.69	No	No	6	No
15 <sup>b</sup>	49	Left kidney	1	55	1,2,3	55	0.35	N.A.	N.A.	N.A.	N.A.

Notes:

a: Case 12 is the remote relapse in a different organ of the same patient as Case 11, after 108 months.

b: Case 15 is a consultation case.

c: Age is taken as the time of operation.

d: 1. Dense lymphoplasmacytic infiltration, 2. Storiform fibrosis, 3. Obliterative phlebitis.

e: Per one high power field on immunohistochemistry.

f: Pre-operative here is defined by one month before the operation.

g: Post-operative here is defined by within 6 months after the operation.

h: Treatment is referred to post-operative steroid and immunosuppressive treatment, Cases 1,2,3 treatment is started after the disease relapsed.

i: Case 1 is a retrospectively diagnosed case. Patient presented as bilateral lacrimal gland enlargement and neck mass in 2004. The disease relapses in left submandibular gland after 24 months. The diagnosis was rendered in 2017 when disease relapsed again. Histological features are based on 2004 resection specimen.

j: Case 2 is a retrospectively diagnosed case. Patient was diagnosed in 2013 when disease relapsed in pancreas, colon and bile duct. Histological features are based on 2008 resection specimen.

k: Case 4 detected aorta and lacrimal gland involvement 4 months after operation. It is not conclusive whether it is a systemic disease or relapse.

l: Case 8 pre-operative serum IgG4 level was measured 2 years before the operation as work-up for the systemic disease.

IgG4-RD: IgG4 related disease; GIST: Gastrointestinal stromal tumor; FNAC: Fine needle aspiration. IMT: Inflammatory myofibroblastic tumour. IPT: Inflammatory pseudotumour, Pred: Prednisolone; MMF: Mycophenolate mofetil; MP: Methylprednisolone; Hc: Hydrocortisone; Rb: Rituximab

Figure 1 - 419

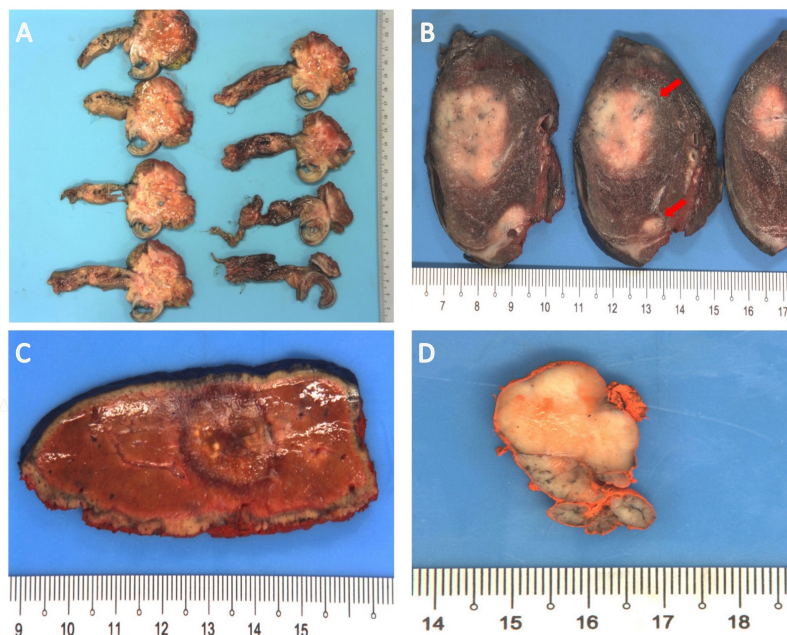
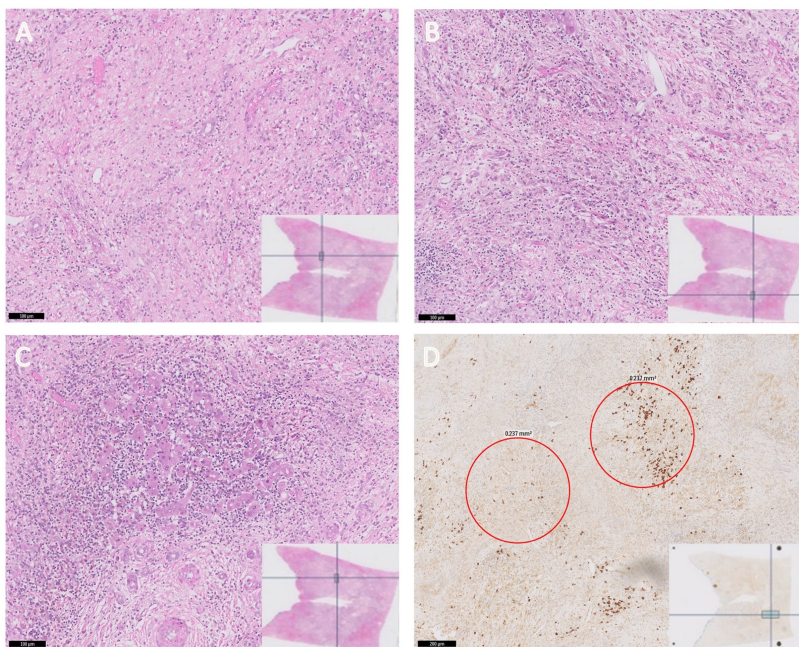


Figure 2 - 419



**Conclusions:** Mass forming IgG4-RD has a male predilection and involves various organ systems. It can be initially misdiagnosed as malignancy and undergo radical resection. The diagnostic histological features of IgG4-RD are readily identified in different organs, however, they are distributed heterogeneously within one lesion. Cases of single organ involvement show an indolent clinical course and normal serum IgG4 level after radical resection.

**420 Immunohistochemical Detection of pan-Tropomyosin Receptor Kinase (pan-TRK) Expression in Solid Tumor Specimens: Inter-Laboratory and Inter-Reader Agreement in NGS-confirmed NTRK Fusion-Positive and Fusion-Negative Cases**

Steven Stratton<sup>1</sup>, Janine Feng<sup>1</sup>, Wen-Wei Liu<sup>1</sup>, Trish Thorne-Nuzzo<sup>1</sup>, Mark Kockx<sup>2</sup>, Frederique Penault-Llorca<sup>3</sup>, Albrecht Stenzinger<sup>4</sup>, Julia Glade<sup>5</sup>, Fernando Lopez-Rios<sup>6</sup>, Esther Conde<sup>6</sup>, Giuseppe Viale<sup>7</sup>, Fernando Soares<sup>8</sup>, Teh-Ying Chou<sup>9</sup>

<sup>1</sup>Roche Tissue Diagnostics, Tucson, AZ, <sup>2</sup>HistoGeneX, Antwerp, Belgium, <sup>3</sup>Centre Jean Perrin, Clermont-Ferrand, France, <sup>4</sup>University of Heidelberg, Ingolstadt, Germany, <sup>5</sup>Institute of Pathology, Heidelberg University Hospital, Heidelberg, Germany, <sup>6</sup>HM Sanchinarro University Hospital-HM Hospitales, Madrid, Spain, <sup>7</sup>University di Milano, Italy, <sup>8</sup>University of Sao Paulo/D'Or Institute of Research, São Paulo, Brazil, <sup>9</sup>Taipei Veterans General Hospital, Taipei, Taiwan

**Disclosures:** Steven Stratton: *Employee, Roche*; Janine Feng: *None*; Wen-Wei Liu: *Employee, Roche Tissue Diagnostics*; Trish Thorne-Nuzzo: *Employee, Roche Tissue Diagnostics*; Mark Kockx: *None*; Frederique Penault-Llorca: *Consultant, Bayer; Grant or Research Support, Bayer; Speaker, Roche; Grant or Research Support, Roche*; Albrecht Stenzinger: *Advisory Board Member, Bayer*; Julia Glade: *None*; Fernando Lopez-Rios: *Grant or Research Support, Roche; Grant or Research Support, Thermo Fisher; Grant or Research Support, Lilly; Speaker, Astra Zeneca; Speaker, Bayer, BMS, ThermoFisher, Lilly, MSD, Pfizer, Roche*; Esther Conde: *Speaker, Roche; Speaker, Pfizer; Speaker, AstraZeneca; Speaker, Merck Sharp & Dohme*; Giuseppe Viale: *Advisory Board Member, Ventana*; Fernando Soares: *None*; Teh-Ying Chou: *None*

**Background:** Neurotrophic Tyrosine Receptor Kinase (*NTRK*) fusions involving *NTRK1*, *NTRK2* and *NTRK3* genes occur in a diverse set of tumors resulting in the constitutive expression of TRK fusion proteins. Wild-type TRK protein expression in most solid tumors is generally minimal. The purpose of this study was to determine the reproducibility of performance of the automated VENTANA pan-TRK (EPR17341) Assay, intended for immunohistochemical detection of the C-terminal region of TRK proteins A, B and C, by assessing interpretations of individual pathologists.



**Design:** This inter-laboratory repeatability study used archived specimens, involving 3 replicate tissue sections from each of 50 next generation sequencing (NGS)-confirmed cases (25 *NTRK* fusion-positive and 25 *NTRK* fusion-negative) for evaluation at 7 independent global sites. Sites were blinded to fusion status of the specimens, which were divided among the sites for staining and then collated for interpretation of digital images. Histologies included colorectal, secretory breast, and salivary gland tumors.

**Results:** Endpoints included between-site and between-reader comparisons of average positive agreement (APA), average negative agreement (ANA), and overall percent agreement (OPA) categorized by intensity and % tumor cell staining in each cellular compartment (membrane, cytoplasm, and nucleus). The derived overall acceptable staining rate was 93.3%. The staining site contributed <0.6% and the reader contributed ≤35.8% to the total variance in the mixed effects model used for analysis of variance in each category. The intraclass correlation coefficient was determined for each scoring category to assess interchangeability between observers, which varied widely. When cases were evaluated in the aggregate for Any Staining (defined as staining above background intensity in ≥1% of tumor cells) vs. No Staining, OPA was 92.6%. In fusion-positive cases the OPA was 92.1%, and in fusion-negative cases the OPA was 93.0%. In specific fusions, OPA ranged from 78.0% (*TPR-NTRK1*, n=1) to 100% (*TPM3-NTRK1* n=3, *LMNA-NTRK1* n=3, and *EML4-NTRK3* n=1). In cases with *ETV6-NTRK3* fusions (n=17), OPA was 88.7%, APA was 93.9%, and ANA was 18.1%.

**Conclusions:** This study provides a framework to assess the inter-reader agreement of the automated VENTANA pan-TRK (EPR17341) Assay in NGS-confirmed *NTRK* gene fusion-positive and fusion-negative cases. Overall agreement between readers was high, but varied based on fusion partner and staining pattern observed with this analytic assay.

**421 Amyloid Typing of Formalin Fixed Paraffin Embedded Tissue by Immunohistochemistry**  
Charitha Vadlamudi<sup>1</sup>, Emily Aniskovich<sup>1</sup>, Hui Chen<sup>1</sup>, Haili Cui<sup>2</sup>, Lawreen Connors<sup>2</sup>, Vaishali Sanchorawala<sup>2</sup>, Eric Burks<sup>3</sup>  
<sup>1</sup>Boston Medical Center, Boston, MA, <sup>2</sup>Boston University, Boston Medical Center, Boston, MA, <sup>3</sup>Boston University Mallory Pathology Associates, Boston, MA

**Disclosures:** Charitha Vadlamudi: None; Emily Aniskovich: None; Hui Chen: None; Haili Cui: None; Lawreen Connors: None; Vaishali Sanchorawala: None; Eric Burks: None

**Background:** The gold standard for amyloid typing is Laser capture microdissection liquid chromatography tandem mass spectrometry (LC MS/MS) or immunoelectron microscopy with gold labelled antibody (IEM). Neither are widely available and both are expensive, generally with long turnaround times. Immunohistochemistry (IHC) is automated, low-cost and faster to perform; however, background staining can be problematic. Herein, we report the optimization and validation of an amyloid-specific immunohistochemical panel for the 4 most common systemic amyloid disease types.

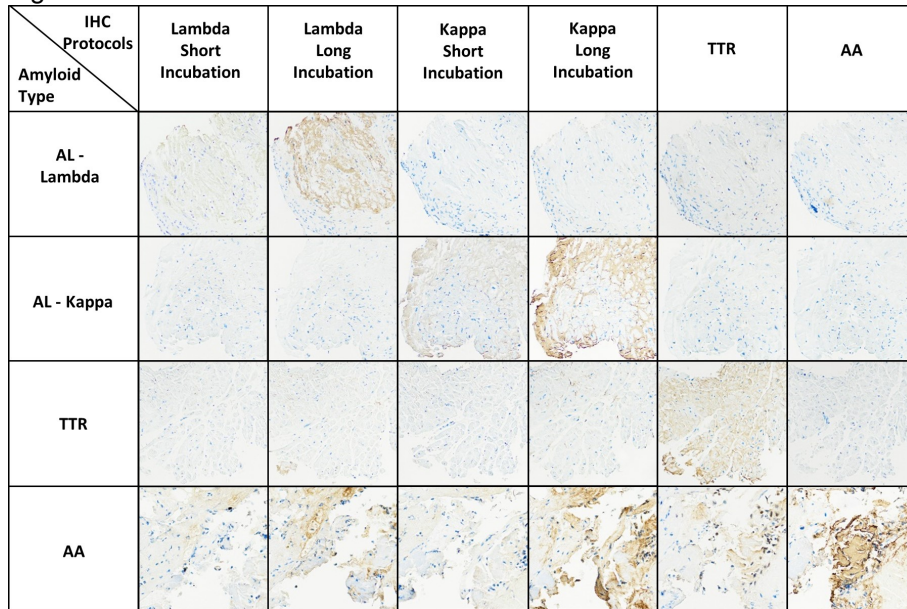
**Design:** FFPE tissue blocks containing amyloid were identified from 60 patients who had undergone amyloid typing by either IEM or LC MS/MS (Table 1). Immunohistochemistry was performed on a Ventana benchmark using Dako/Agilent antibodies directed against AA (monoclonal mouse anti-human amyloid A M0759), TTR (polyclonal rabbit anti-human prealbumin/TTR, A000202-2), Immunoglobulin (Ig) light chain (LC)-kappa (polyclonal rabbit anti-human kappa LC A019102-2) and IgLC-lambda (polyclonal rabbit anti-human lambda LC A019302-2).

**Results:** A total of 60 cases were stained with 6 immunohistochemical stains; these included AA, TTR, LC-lambda and LC-kappa, with the latter two tested at both short (12-24 minute) and long (60-120 minute) incubation times. Overall, 53 of the 60 cases (88%) were definitively typed by IHC; these included 100%, 95%, 88%, and 76% of AA, ATTR, AL (kappa), and AL (lambda) cases, respectively (Table 1). Sensitivity of IHC testing by amyloid type was 100% for AA, ATTR and AL-lambda using the long incubation protocol; sensitivity in AL-kappa cases using an extended incubation time was 94%. The intensity of staining was moderate to strong in the majority of tested samples. While a shorter incubation time in LC-kappa and -lambda cases demonstrated minimal background staining, lower sensitivities (59% and 71%, respectively) and weaker staining intensities (Figure 1) but higher specificity (Table 1).

Table 1: Distribution of IHC results among amyloid subtypes.

	<b>AA</b>	<b>ATTR</b>	<b>AL-kappa</b>	<b>AL-lambda</b>
<b>Total Cases, N</b>	7	19	17	17
<b>AA</b>	7 (100%)	0	1 (6%)	1 (6%)
<b>ATTR</b>	0	19 (100%)	0	2 (12%)
<b>AL-kappa (Short)</b>	0	0	10 (59%)	1 (6%)
<b>AL-kappa (Long)</b>	0	1 (5%)	16 (94%)	2 (12%)
<b>AL-lambda (Short)</b>	0	0	0	12 (71%)
<b>AL-lambda (Long)</b>	0	1 (5%)	0	17 (100%)
<b>Definitive IHC Amyloid Protein Identification</b>	7 (100%)	18 (95%)	15 (88%)	13 (76%)

Figure 1 - 421



**Conclusions:** A well validated IHC panel for amyloid typing allows for rapid and cost-effective amyloid protein identification in the majority (88%) of cases tested in the current study. We suggest that the majority of systemic amyloid cases can be successfully typed using IHC analyses, while a smaller number demonstrating indeterminate IHC results and those associated with rarer amyloid disease forms may be triaged for LC MS/MS or IEM testing.